AIAA SciTech Forum
January 3-7, 2022, San Diego, CA & Virtual
AIAA SCITECH 2022 Forum

10.2514/6.2022-2274

Minimum-Fuel LEO-to-MEO Orbit Transfer Using Multi-Domain Gaussian Quadrature Collocation

Brittanny V. Holden,* and Anil V. Rao†

Department of Mechanical and Aerospace Engineering
University of Florida
Gainesville, FL 32611-6250

A numerical optimization study of a minimum-fuel LEO-to-MEO orbital trajectory transfer is solved using a bang-bang and singular optimal control (BBSOC) method with multi-domain Legendre-Gauss-Radau quadrature collocation. Modified equinoctial elements are used to avoid singularities that occur in orbital elements. The time, t, state components, (p, f, g, h, k, L, m), and control components, (u_r, u_t, u_n, T) are optimized in this one phase problem where seven cases of the initial thrust acceleration values are considered. The structure of the thrust was not assumed, therefore the optimizer determined the number of switch points. The solutions were categorized as partial and multiple revolution optimal trajectories. The initial thrust accelerations considered for the partial revolution solutions are $s_0 = \left[1.0206 \times 10^{0}, 5.1029 \times 10^{-1}, 1.0206 \times 10^{-1}, 5.1029 \times 10^{-2}\right]$ AU. Furthermore, as the initial thrust acceleration decreased, the final mass decreased while the total time thrusting increased. The initial thrust accelerations considered for the multiple revolution solutions are $s_0 = \left[1.0206 \times 10^{-2}, 5.1029 \times 10^{-3}, 1.0206 \times 10^{-3}\right]$ AU. Furthermore, as the initial thrust acceleration decreased, the final mass increased while the total time thrusting increased. An in-depth study was completed for the cases of $s_0 = \left[1.0206 \times 10^{-1}, 1.0206 \times 10^{-3}\right]$ AU, where the final mass was $[0.6683, 0.5991]$ MU and the total time thrusting was $[4.0305, 487.3276]$ TU.

Nomenclature

a	semi-major axis
AU	acceleration unit
DU	length unit
e	eccentricity
f	second modified equinoctial orbital element
FU	force unit
g	third modified equinoctial orbital element
g_E	sea level gravity of Earth
h	fourth modified equinoctial orbital element
i	inclination
I_{sp}	specific impulse
k	fifth modified equinoctial orbital element
L	true longitude

*Ph.D. Student, Department of Mechanical and Aerospace Engineering, University of Florida. Phone: 904-238-1746. E-mail: brittanny-holden@ufl.edu

†Professor, Department of Mechanical and Aerospace Engineering, University of Florida. Associate Fellow AIAA. Corresponding Author. Phone: 352-672-1529. E-mail: anilvrao@ufl.edu

m	mass of spacecraft
m_0	initial mass of spacecraft
$\dot{m}$	mass flow rate
MU	mass unit
p	semi-latus rectum (first modified equinoctial orbital element)
r	distance from Earth to spacecraft
R_E	radius of Earth
s_0	initial thrust acceleration
t	time
t_0	initial time
t_f	terminal time
t_{Thrust}	total time thrusting
T	thrust magnitude
TU	time unit
$T_{\max}$	maximum thrust magnitude
VU	speed unit
u_r	radial component of thrust direction
u_t	transverse component of thrust direction
u_n	normal component of thrust direction
μ_E	gravitational parameter of Earth
ν	true anomaly
ω	argument of periapsis
Ω	right ascension of the ascending node

I. Introduction

For several decades, a topic of interest to the space community has been studying and advancing propulsion technology. Traditionally, high-thrust chemical propulsion was used for space travel, but more recently has been replaced with low-thrust propulsion, using either electric propulsion or solar electric propulsion, due to high propellant efficiencies that can reduce the cost of missions. Using a low-thrust propulsion system has a significantly lower fuel consumption than a high-thrust propulsion system, though the propulsion system is typically in use for a significant portion of the mission and can result in a longer duration for the completion of the mission. This research focuses on the use of a variety of low-thrust propulsion values to accomplish an orbit transfer from a low-Earth orbit (LEO) to a middle-Earth orbit (MEO).

Much exploration and investigation has been conducted previously on the design of low-thrust orbital transfer missions [1–11]. Ref. [1] conducted a survey on approaches for low-thrust trajectory optimization and focused on being able to solve hybrid-optimal control problems. Extensive research went into the review of traditional and new methodologies and tools and it was determined that most low-thrust trajectory optimizers are complicated, not easily able to include mission-planning, and cannot search over multi-objective design spaces. Ref. [2] compared two nonlinear model predictive control strategies to solve a minimum-fuel Earth-to-Mars rendezvous maneuver to showcase the ability to use each strategy to solve problems with interplanetary orbital dynamics and low control authority. The first strategy consisted of solving the optimal control problem over a receding horizon with a fixed number of control subintervals and was able to withstand errors in control allocation and unmodeled effects. The second strategy consisted of solving the optimal control problem over a receding horizon with a shrinking number of control subintervals. Then, in order to maintain controllability, a doubling strategy was employed and was shown to also handle more complicated bounded

problems as well. Ref. [3] developed a novel method, called evolutionary neurocontrollers, to solve low-thrust orbital transfer optimal control problems that combines evolutionary algorithms and artificial neural networks. The benefit of this method is that it does not require an initial guess because most traditional local optimizers have a convergence behavior that depends heavily on an adequate initial guess, so the solution obtained is usually close to the initial guess. Ref. [4] implemented a homotopic approach to solve a minimum-fuel low-thrust optimal trajectory problem, which decreased the computational time and increased the chance of determining the global optimal solution. The switching structure is also detected by finding the first and second-order time derivatives of the switching function to determine if the control is bang-bang. Refs. [5, 6] both implement genetic algorithms to obtain solutions to low-thrust orbit trajectory optimal control problems. Ref. [5] investigated the effectiveness of genetic algorithms to determine near-optimal low-thrust trajectory solutions with the ability to implement a thrust/coast arc variable, whereas Ref. [6] used a hybrid optimization method that consisted of a multi-objective genetic algorithm with a low-thrust trajectory optimizer that implemented calculus of variations. Ref. [7] focused on determining high-accuracy solutions for a minimum-time, low-thrust Earth-orbit transfer problem using a variable-order Legendre-Gauss-Radau collocation method. An initial guess was generated by solving a sequence of modified optimal control problems one-revolution at a time until the terminal boundary conditions were satisfied. Ref. [8] optimized a low-thrust orbit transfer problem with eclipsing, where the spacecraft is on a coasting arc when passing through Earth's shadow and used a receding horizon algorithm to create an initial guess. The optimal control problem was separated into multiple phases based on the thrust structure. Ref. [9] solved a minimum-fuel low-thrust Earth-to-Mars orbital transfer using both indirect and direct methods assuming a on-off-on thrust structure. For the indirect method, a two-point boundary value problem was derived, whereas for the direct method, an optimal control software $\mathbb{GPOPS}-\mathbb{II}$ was used to solve the optimal control problem. Ref. [10] solved a minimum-fuel low-thrust orbital transfer problem where the thrust is discontinuous with a homotopic method, in order to establish convergence properties, where 1786 switches were detected for a thrust of 0.1 N.

This research is inspired by the work of Ref. [11]. While both this work and Ref. [11] focus on the design of a minimum-fuel Earth-centric orbit transfer using low thrust propulsion, the works vary significantly from one another. First, the research in this work is focused only on a LEO-to-MEO orbit transfer, whereas Ref. [11] also studies LEO-to-HEO and LEO-to-GEO transfers. Second, this work is solved using a method for solving bang-bang and singular optimal control problems using multi-domain Legendre-Gauss-Radau collocation as described in Ref. [12] and the nonlinear programming (NLP) problem solver *IPOPT* as described in Ref. [13], whereas Ref. [11] uses a direct higher order collocation 7th degree system (DHOC7) as described in Ref. [14] and the NLP problem solver *SNOPT*. Third, this work uses the components of the thrust direction as the control in order to negate the possibility of the wrapping effect that can occur from using angles as the control, whereas Ref. [11] used the in-plane and out-of-plane thrust angle as the control. Fourth, this work studied seven cases of initial thrust acceleration, $s_0 = \left[1.0\times10^{1}, 5.0\times10^{0}, 1.0\times10^{0}, 5.0\times10^{-1}, 1.0\times10^{-1}, 5.0\times10^{-2}, 1.0\times10^{-2}\right]$ $\mathrm{m}\cdot\mathrm{s}^{-2}$, whereas Ref. [11] studied four cases, $s_0 = \left[1.0\times10^{1}, 1.0\times10^{0}, 1.0\times10^{-1}, 1.0\times10^{-2}\right]$ $\mathrm{m}\cdot\mathrm{s}^{-2}$. Fifth, this work did not assume the thrusting structure and allowed our method to determine the optimal thrusting structure, whereas Ref. [11] determined a burn-coast-burn thrusting structure a priori that is modeled after the burn structure described in Ref. [15].

This paper is as organized as follows. Section II presents the one-phase minimum-time LEO-to-MEO orbital transfer optimal control problem by providing the modeling assumptions, dynamics, path constraints, event constraints, the units used to solve the problem, boundary conditions, and variable bounds. Section III presents the results and discussion of the numerical optimization study using the MATLAB optimal control software, $\mathbb{GPOPS}-\mathbb{II}$. Section IV presents the conclusions on this research.

II. Problem Description

This section develops the assumptions, equations of motion, constraints, and boundary conditions that define the LEO-to-MEO orbit transfer optimal control problem. Section II.A presents the simplifications and assumptions that were used to model the motion of the spacecraft. Section II.B provides the differential equations of motion for the spacecraft as well as the path constraints and event constraints. Section II.C presents the units used to solve the problem. Section II.D presents the initial and terminal boundary conditions as well as the lower and upper bounds on the time, control, and state in each phase. Finally, a description of the complete optimal control problem is provided in Section II.E.

A. Modeling Assumptions

First, it is assumed that the spacecraft is modeled as a point mass. Second, the only forces acting on the spacecraft are those due to thrust and spherical two-body gravity between the spacecraft and the Earth. Consequently, third-body effects and zonal harmonic gravitational coefficients are neglected. Third, the control is the thrust direction, $\mathbf{u} = (u_r, u_t, u_n)$, and magnitude, T. Finally, when the eccentricity is zero, $e = 0$, the argument of periapsis is undefined, therefore it is assumed that $\omega = 0$ rad.

B. Equations of Motion

The dynamics of the spacecraft are described using modified equinoctial elements, $(p(t), f(t), g(t), h(t), k(t), L(t))$, and the mass, $m(t)$. The first modified equinoctial element, p, is the semi-latus rectum, the second and third modified equinoctial elements, f and g, describe the eccentricity, e, of the orbit, the fourth and fifth modified equinoctial elements, h and k, describe the inclination, i, of the orbit, and the sixth modified equinoctial element, L, is the true longitude. The differential equations of motion of the spacecraft are given as [16]

$$\begin{aligned}
\frac{dp}{dt} &= \sqrt{\frac{p}{\mu_E}}\frac{2p}{w}\Delta_t, \\
\frac{df}{dt} &= \sqrt{\frac{p}{\mu_E}}\left[\sin L\Delta_r + \frac{1}{w}\left[(w+1)\cos L + f\right]\Delta_t - \frac{g}{w}\left(h\sin L - k\cos L\right)\Delta_n\right], \\
\frac{dg}{dt} &= \sqrt{\frac{p}{\mu_E}}\left[-\cos L\Delta_r + \frac{1}{w}\left[(w+1)\sin L + g\right]\Delta_t + \frac{g}{w}\left(h\sin L - k\cos L\right)\Delta_n\right], \\
\frac{dh}{dt} &= \sqrt{\frac{p}{\mu_E}}\frac{q^2}{2w}\cos L\Delta_n, \\
\frac{dk}{dt} &= \sqrt{\frac{p}{\mu_E}}\frac{q^2}{2w}\sin L\Delta_n, \\
\frac{dL}{dt} &= \sqrt{\mu_E p}\left(\frac{w}{p}\right)^2 + \frac{1}{w}\sqrt{\frac{p}{\mu_E}}\left(h\sin L - k\cos L\right)\Delta_n, \\
\frac{dm}{dt} &= -\frac{T}{g_E I_{sp}},
\end{aligned} \tag{1}$$

where

$$\begin{aligned}
q^2 &= 1 + h^2 + k^2, \\
w &= 1 + f\cos L + g\sin L.
\end{aligned} \tag{2}$$

The non-two-body perturbations in the radial, transverse, and normal directions, $(\Delta_r, \Delta_t, \Delta_n)$, are due to the thrust of the spacecraft and are given as

$$\begin{aligned}
\Delta_r &= \frac{T}{m}u_r, \\
\Delta_t &= \frac{T}{m}u_t, \\
\Delta_n &= \frac{T}{m}u_n.
\end{aligned} \tag{3}$$

The control consists of the thrust magnitude, T, and the thrust direction, $\mathbf{u} = (u_r, u_t, u_n)$, where the radial direction is along the Earth-spacecraft line, the transverse direction is along the orbital motion and perpendicular to the radial vector, and the normal direction is along the orbit's angular momentum vector. Next, in order to ensure that the thrust direction is a unit vector, the following equality path constraint is enforced:

$$u_r^2 + u_t^2 + u_n^2 = 1 \tag{4}$$

Finally, in order to ensure that the final orbit is achieved, the following terminal event constraints are enforced, which are modeled after Ref. [17]:

$$\begin{aligned} p\left(t_f\right) &= a_f\left(1-e_f^2\right), \\ f^2\left(t_f\right)+g^2\left(t_f\right) &= e_f^2, \\ h^2\left(t_f\right)+k^2\left(t_f\right) &= \tan^2\left(\frac{i_f}{2}\right), \\ k\left(t_f\right) &= \sin\left(\Omega_f\right), \\ h\left(t_f\right) &\geq 0, \end{aligned} \tag{5}$$

where only the terminal semi-major axis, a_f, eccentricity, e_f, inclination, i_f, and right ascension of the ascending node, Ω_f, are constrained because the MEO eccentricity is 0, which means that the argument of periapsis, $\omega\left(t_f\right)$, is undefined, and the true anomaly, $\nu\left(t_f\right)$, is considered to be free. The numerical values of the variables required to model and solve the problem are given in Table 2.

Table 2 Physical constants.

Quantity	Value	Units
Earth Radius, R_E	6.378145×10^6	m
Earth Gravitational Parameter, μ_E	$3.986004418 \times 10^{14}$	$\mathrm{m}^3 \cdot \mathrm{s}^{-2}$
Earth Sea Level Gravity, g_E	9.80665×10^5	$\mathrm{m} \cdot \mathrm{s}^{-2}$
Initial Mass, m_0	1.000×10^3	kg
Specific Impulse, I_{sp}	1.000×10^3	s

C. Scale Factors

The units used in the optimal control problem were chosen such that the gravitational parameter of the Earth is equal to unity. In order to attain a gravitational parameter of unity, the distance unit, DU, speed unit, VU, time unit, TU, acceleration unit, AU, mass unit, MU, and force unit, FU, were chosen as follows:

$$\begin{bmatrix} \mathrm{DU} \\ \mathrm{VU} \\ \mathrm{TU} \\ \mathrm{AU} \\ \mathrm{MU} \\ \mathrm{FU} \end{bmatrix} = \begin{bmatrix} R_E \\ \sqrt{\mu_E/\mathrm{DU}} \\ \mathrm{DU}/\mathrm{VU} \\ \mathrm{VU}/\mathrm{TU} \\ m_0 \\ \mathrm{MU} \cdot \mathrm{AU} \end{bmatrix}. \tag{6}$$

D. Boundary Conditions and Bounds

Table 3 shows the orbital elements of the initial low Earth orbit and terminal middle Earth orbit obtained from Ref. [11]. Bounds are placed on the true longitude, control, and state and are given as

Table 3 Orbital elements for LEO and MEO orbits.

Orbital Element	LEO	MEO
Semi-major Axis, a	7.003×10^6 (m) = 1.0980 (DU)	2.656×10^7 (m) = 4.1642 (DU)
Eccentricity, e	0	0
Right Ascension of the Ascending Node, Ω (rad)	0	0
Inclination, i (rad)	0.4974	0.9547
Argument of Periapsis, ω (rad)	Undefined (Chosen to be 0)	Undefined
True Anomaly, ν (rad)	Free	Free

$$
\begin{aligned}
t_{0,\min} &\le t_0 \le t_{0,\max} \\
t_{f,\min} &\le t_f \le t_{f,\max} \\
u_{r,\min} &\le u_r \le u_{r,\max} \\
u_{t,\min} &\le u_t \le u_{t,\max} \\
u_{n,\min} &\le u_n \le u_{n,\max} \\
T_{\min} &\le T \le T_{\max} \\
p_{\min} &\le p \le p_{\max} \\
f_{\min} &\le f \le f_{\max} \\
g_{\min} &\le g \le g_{\max} \\
h_{\min} &\le h \le h_{\max} \\
k_{\min} &\le k \le k_{\max} \\
L_{\min} &\le L \le L_{\max} \\
m_{\min} &\le m \le m_{\max}
\end{aligned}
\quad . \tag{7}
$$

Table 4 provides the initial and terminal boundary conditions along with the lower and upper bounds. Table 5 gives the initial thrust acceleration, s_0, and the maximum thrust magnitude, $T_{\max}$, for all cases studied in this research.

Table 4 Initial and terminal boundary conditions with lower and upper bounds.

Variable	Initial	Terminal	[Lower, Upper]
Time, t (TU)	0	Free	[0, Free]
Radial Thrust Direction, u_r	Free	Free	[Free, Free]
Transverse Thrust Direction, u_t	Free	Free	[Free, Free]
Normal Thrust Direction, u_n	Free	Free	[Free, Free]
Thrust Magnitude, T (FU)	Free	Free	$[0, T_{\max}]$
Semi-latus Rectum, p (DU)	1.0980	4.1642	[Free, Free]
Second Modified Equinoctial Element, f	0	Free	$[-1, 1]$
Third Modified Equinoctial Element, g	0	Free	$[-1, 1]$
Fourth Modified Equinoctial Element, h	0.2540	Free	$[-1, 1]$
Fifth Modified Equinoctial Element, k	0	Free	$[-1, 1]$
True Longitude, L (rad)	Free	Free	[Free, Free]
Mass, m (MU)	1	Free	[0.01, 1]

Table 5 Initial thrust acceleration and maximum thrust values for all cases.

Initial Thrust Acceleration, s_0		Maximum Thrust, $T_{\max}$	
$\left(\mathrm{m}\cdot\mathrm{s}^{-2}\right)$	(AU)	(N)	(FU)
1.0×10^{1}	1.0206×10^{0}	1.0×10^{4}	1.0206×10^{0}
5.0×10^{0}	5.1029×10^{-1}	5.0×10^{3}	5.1029×10^{-1}
1.0×10^{0}	1.0206×10^{-1}	1.0×10^{3}	1.0206×10^{-1}
5.0×10^{-1}	5.1029×10^{-2}	5.0×10^{2}	5.1029×10^{-2}
1.0×10^{-1}	1.0206×10^{-2}	1.0×10^{2}	1.0216×10^{-2}
5.0×10^{-2}	5.1029×10^{-3}	5.0×10^{1}	5.1029×10^{-3}
1.0×10^{-2}	1.0206×10^{-3}	1.0×10^{1}	1.0216×10^{-3}

E. Optimal Control Problem

For the LEO-to-MEO Earth orbit transfer, the optimal control problem is stated as follows. Determine the state (p, f, g, h, k, L, m), the control (u_r, u_t, u_n, T), as well as the terminal time t_f which maximizes the final mass of the spacecraft, m_f, therefore the following cost functional needs to be minimized

$$J = -m_f \tag{8}$$

while satisfying the dynamics and path constraints in Section II.B and the variable bounds and boundary conditions in Section II.D.

III. Results and Discussion

This section presents the results acquired by solving the LEO-to-MEO orbital transfer optimal control problem described in Section II. This problem is solved for multiple initial thrust acceleration values. It is noted that only the cases of $s_0 = \left[1.0206\times10^{-1}, 1.0206\times10^{-3}\right]$ AU are studied in-depth and are presented in Subsection III.B.1 and Subsection III.B.2, respectively. The LEO-to-MEO orbital transfer problem is solved using the general-purpose MATLAB optimal control software $\mathbb{GPOPS}-\mathbb{II}$ [18] with the following settings.

First, the bang-bang and singular optimal control (BBSOC) method described in Ref. [12] is used to detect the structure of the solution and solve the optimal control problem. This method solves bang-bang and singular optimal control problems using multi-domain Legendre-Gauss-Radau (LGR) collocation. The structure detection portion of the BBSOC method locates the switch times in the control, and then determines where the solution is bang-bang or singular by inspecting the corresponding switching function. Once the structure has been detected, the problem is split into multiple domains such that it includes additional decision variables that represent the switch points in order to optimize the location of the non-smooth portions of the control. It is noted that the control is set to either the upper or lower limit for bang-bang domains. Second, the mesh refinement method described in Ref. [19] is used with a mesh refinement accuracy tolerance, ϵ_{mesh}, of 10^{-5}. This method solves a continuous-time optimal control problem using collocation at LGR points and allows for changes in the number of mesh intervals and the degree of the approximating polynomial within the mesh interval. During this process, the degree of the polynomial within a specified mesh interval is increased if the degree is below the maximum allowable degree and if the degree is above the maximum allowable degree, the mesh interval is divided into sub-intervals. Third, the nonlinear program (NLP) solver *IPOPT* [13] is employed in full Newton (second derivative) mode with an NLP solver tolerance, ϵ_{NLP}, of 10^{-6}. All first and second derivatives required by *IPOPT* ware obtained using ADiGator, an open-source algorithmic differentiation software [20]. Finally, all computations were performed using a 2.9 GHz Intel Core i9 MacBook Pro running Mac OS version 11.6 (Big Sur) with 32GB 2400MHz DDR4 RAM and MATLAB Version R2018b (build 9.5.0.944444).

In order to solve the minimum-fuel LEO-to-MEO optimal control problem described in Section II, an initial guess must be supplied to $\mathbb{GPOPS}-\mathbb{II}$. In this research, the initial guess is determined for each case by using the ordinary differential equations solver *ode*113 in MATLAB. The ODE solver is used to integrate the spacecraft dynamics, $(p(t), f(t), g(t), h(t), k(t), L(t), m(t))$, in Eq. (1) with the initial conditions given as the LEO orbital elements in Table 3 that are then converted to modified equinoctial elements. The initial guess is integrated until the semi-major

axis, a, of the orbit is equal to the corresponding MEO value, $a_f = 4.1642$ DU. For the control, (u_r, u_t, u_n, T), the thrust magnitude, T, is considered to be at maximum for the entirety of the integration and the thrust direction components are solved for afterwards by assuming that the thrust is always in the same direction as the velocity vector. It is noted in this study that the minimum-fuel LEO-to-MEO orbit transfer optimal control problem is solved using initial thrust acceleration values in Table 5, which are inspired by the values given in Ref. [11]. The key features of the solutions are shown for the cases of $s_0 = \left[1.0206 \times 10^{-1}, 1.0206 \times 10^{-3}\right]$ AU.

A. Overall Performance

The minimum-fuel results for the LEO-to-MEO transfer for multiple initial thrust acceleration values are shown in Table 6. For each case of s_0, the final mass, m_f, fuel consumed, $m_0 - m_f$, total thrusting time, t_{Thrust}, total number of revolutions, and the number of thrust arcs are presented. The solutions can be separated into two categories: orbital trajectories with partial revolutions and multiple revolutions. The cases with partial revolutions are $s_0 = \left[1.0206 \times 10^{0}, 5.1029 \times 10^{-1}, 1.0206 \times 10^{-1}, 5.1029 \times 10^{-2}\right]$ AU. As the initial thrust acceleration decreases, the final mass decreases, while naturally the amount of fuel consumed increases, and the total time thrusting increases. During these cases, the final mass decreases with respect to decreasing initial thrust acceleration values because the thrust arcs occur for a longer period of time, where the largest value of $s_0 = 1.0206 \times 10^{0}$ AU has a total thrusting time of $t_{Thrust} = 0.3784$ TU, whereas the smallest value of $s_0 = 5.1029 \times 10^{-2}$ AU has a total thrusting time of $t_{Thrust} = 12.4948$ TU. An interesting phenomenon occurs for the four largest values of initial thrust acceleration. Specifically, the three largest cases only have two thrust arcs while the fourth largest initial thrust acceleration, $s_0 = 5.1029 \times 10^{-2}$ AU, has a partial revolution with only one thrust arc.

The cases with multiple revolutions are $s_0 = \left[1.0206 \times 10^{-2}, 5.1029 \times 10^{-3}, 1.0206 \times 10^{-3}\right]$ AU. As the initial thrust acceleration decreases, the final mass increases, while naturally the amount of fuel consumed decreases, and the total time thrusting increases. During these cases, the final mass increases with respect to decreasing initial thrust acceleration values because the spacecraft was either thrusting continuously, as in $s_0 = \left[1.0206 \times 10^{-2}, 5.1029 \times 10^{-3}\right]$ AU, or has only short coasting arcs, as in $s_0 = 1.0206 \times 10^{-3}$ AU, therefore a smaller initial thrust acceleration value would consume the least fuel, even though a smaller s_0 occurs over a larger time period. The total number of revolutions needed to complete the orbit transfer increases, which is expected behavior when decreasing the initial thrust acceleration values, with the exception of $s_0 = 5.1029 \times 10^{-1}$ AU that completes 0.5352 revolutions for the optimal trajectory, whereas $s_0 = 1.0206 \times 10^{0}$ AU completes 0.6150 revolutions for the optimal trajectory. This behavior is due to the smaller initial thrust acceleration value leading to a longer total time thrusting, while consuming almost the same amount of fuel, where the consumption differs by 0.0002 MU.

Table 6 Final mass, fuel consumption, total time thrusting, total revolutions, and thrust arcs.

s_0 (AU)	m_f (MU)	$m_0 - m_f$ (MU)	t_{Thrust} (TU)	Total Revolutions	Thrust Arcs
1.0206×10^{0}	0.6750	0.3250	0.3784	0.6150	2
5.1029×10^{-1}	0.6748	0.3252	0.7800	0.5352	2
1.0206×10^{-1}	0.6683	0.3317	4.0305	0.6774	2
5.1029×10^{-2}	0.4860	0.5140	12.4948	0.8328	1
1.0206×10^{-2}	0.5728	0.4272	51.9162	3.8895	1
5.1029×10^{-3}	0.5929	0.4071	98.8230	13.3663	1
1.0206×10^{-3}	0.5991	0.4009	487.3276	31.6368	4

B. Key Features of Optimized Solutions

This section shows the key features of the partial revolution optimal trajectory solutions using the particular case of $s_0 = 1.0206 \times 10^{-1}$ AU and of the multiple revolution optimal trajectory solutions using the particular case of $s_0 = 1.0206 \times 10^{-3}$ AU. The results shown focus on the spacecraft trajectory and the control that produces the observed behavior. It is noted that in all figures, the solid red line represents when the spacecraft is on a coasting arc.

1. Partial Revolution Optimized Solution

Figure 1 shows the optimized three-dimensional trajectory of the LEO-to-MEO transfer for $s_0 = 1.0206 \times 10^{-1}$ AU in scaled Cartesian coordinates, where the conversion between modified equinoctial elements and position can be found in Ref. [16]. It is seen that the spacecraft begins in a low Earth orbit that corresponds to the orbital elements $(a_0, e_0, \Omega_0, i_0, \omega_0, \nu_0) = (1.0980 \text{ DU}, 0, 0 \text{ rad}, 0.4974 \text{ rad}, 0 \text{ rad}, \text{Free})$ and terminates in a middle Earth orbit that corresponds to the orbital elements $\left(a_f, e_f, \Omega_f, i_f, \omega_f, \nu_f\right) = (4.1642 \text{ DU}, 0, 0 \text{ rad}, 0.9547 \text{ rad}, \text{Undefined}, \text{Free})$. The optimal trajectory consists of 0.6774 revolutions with a final mass of 0.6683 MU, two thrust arcs, and a total time thrusting of 4.0305 TU. It is seen that the spacecraft begins and ends with a thrust arc.

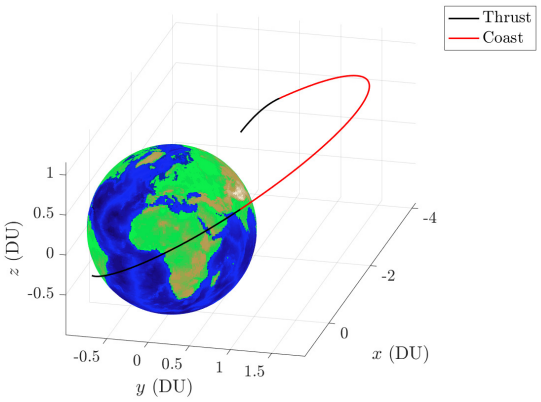

Fig. 1 Optimal three-dimensional spacecraft trajectory.

Figure 2 shows the behavior of the orbital elements of the optimized trajectory. The semi-major axis, a, increases from 1.0980 DU to 2.6684 DU during the first thrust arc, remains at 2.6684 DU for the duration of the coast arc, then increases to 4.1642 DU during the final thrust arc. The semi-major axis is always increasing because the trajectory of the spacecraft is always moving farther away from the Earth. The eccentricity, e, increases steadily from 0 to 0.5592 during the first thrust arc, remains at 0.5592 for the duration of the coast arc, and then decreases to 0 during the final thrust arc. The eccentricity begins and ends at 0 because the initial and terminal orbits are circular, and rapidly changes during the thrust arcs because the optimal trajectory changes from circular to increasingly more elliptic then back to circular in order to maximize the final mass. The right ascension of the ascending node, Ω, begins at 0 rad, decreases to -0.0227 rad, then increases to 0.0057 rad during the first thrust arc, remains at 0.0057 rad during the coast arc, and then decreases to -0.0097 rad and increases to 0 rad. This behavior is a result of the boundary conditions for both the initial LEO and final MEO orbit, since it is required that $\Omega = 0$ rad at those points on the trajectory. It is also noted that the line of nodes moves only slightly since Ω has a range of 0.0284 rad. The inclination, i, slowly increases from 0.4974 rad to 0.5442 rad during the first thrust arc, remains at 0.5442 rad during the coast arc, and then rapidly increases to 0.9547 rad during the final thrust arc. The inclination changes by 0.0468 rad during the first thrust arc and by 0.4105 rad during the final thrust arc. The maneuvers are more fuel efficient because the spacecraft is farther away from the Earth, therefore the velocity is smaller, and inclination changes require a change in the direction of velocity. Therefore, when the velocity is smaller the maneuver will require less fuel to be implemented, so the inclination changes more during the final thrust arc. The argument of the periapsis, ω, is only undefined at the initial and terminal end points because $e = 0$, which explains the discontinuities that occurs at the beginning and end of the trajectory. For the defined portions of ω, it starts at -0.9608 rad then increases to -0.0144 rad during the first thrust arc, remains at -0.0144 rad during the coast arc, then increases to 0.0735 rad during the final thrust arc. The true longitude, L, rapidly increases from -1.0266 rad to 1.0038 rad during the first thrust arc, increases from 1.0038 rad to 3.0666 rad during the coast arc, and then slowly increases to 3.2294 rad during the final thrust arc. It is noted that the true longitude rapidly increases during the first thrust arc compared to the slow increase during the final thrust arc because the velocity of the spacecraft is higher when it is located closer to Earth.

Figure 3 shows the mass of the spacecraft throughout the fuel-optimized trajectory. The mass starts at 1 MU, as in accordance with the initial boundary conditions, then decreases to 0.8057 MU during the first thrust arc, remains at 0.8057 MU during the coast arc, and then decreases to 0.6683 MU during the final thrust arc, which is the optimized final mass. The amount of fuel consumed for the LEO-to-MEO transfer is 0.3317 MU.

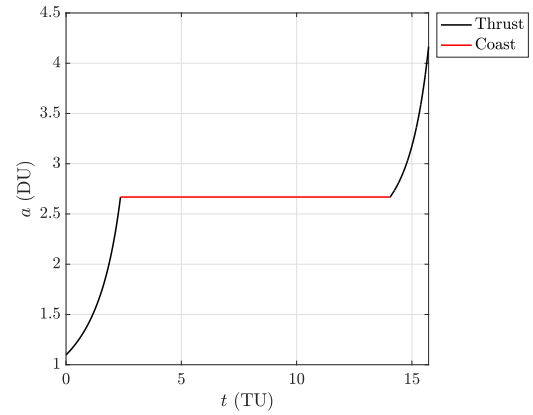

(a) Semi-major axis.

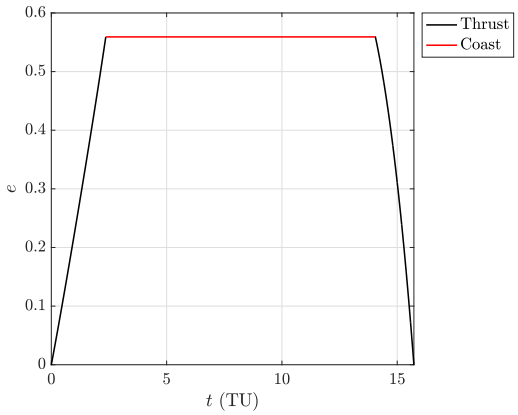

(b) Eccentricity.

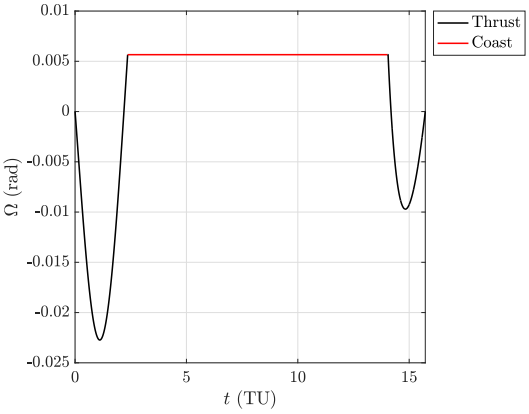

(c) Right ascension of the ascending node.

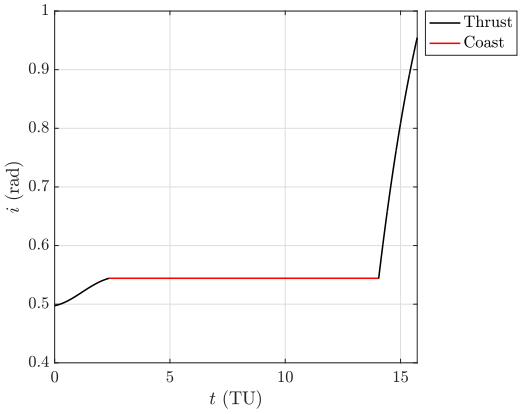

(d) Inclination.

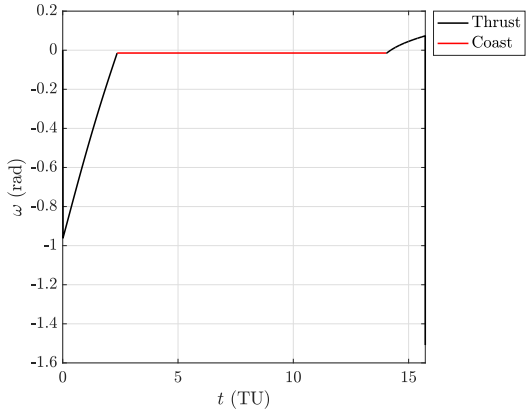

(e) Argument of the periapsis.

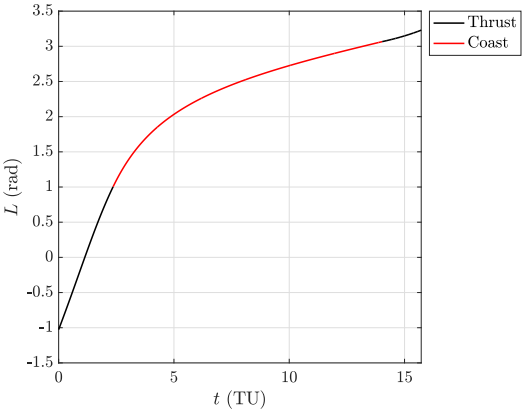

(f) True longitude.

Fig. 2 Orbital elements of the optimal trajectory.

Finally, Fig. 4 shows the control components of the optimal trajectory, which are the thrust magnitude, T, and the thrust direction components, (u_r, u_t, u_n). The thrust magnitude starts at $T_{\max} = 0.1021$ FU, decreases to 0 FU on the coast arc, and then increases to $T_{\max} = 0.1021$ FU, therefore the thrust has two discontinuities and the structure of this solution is bang-off-bang. It is noted that the structure of the thrust is not assumed before solving the problem. The

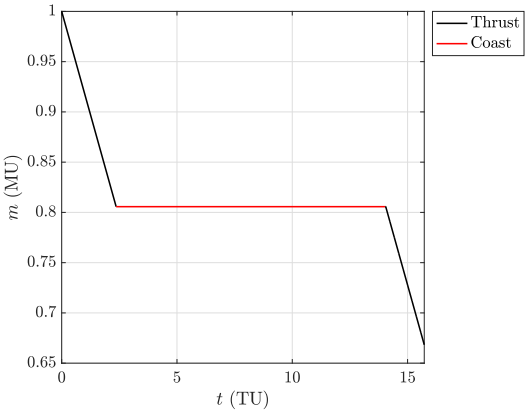

Fig. 3 Mass of spacecraft.

components of the thrust direction are only applicable when the thrust is non-zero (i.e., the two thrust arcs). The radial thrust direction, u_r, increases from -0.1187 to 0.3080 during the first thrust arc, and then decreases from 0.0278 to 0.0133 to then increase to 0.0237 during the final thrust arc. The transverse thrust direction, u_t, decreases from 0.9812 to 0.9383 during the first thrust arc, and then increases from 0.5374 to 0.8276 during the final thrust arc. The normal thrust direction, u_n, increases from 0.1520 to 0.2365 then decreases to 0.1572 during the first thrust arc, and then increases from -0.8429 to -0.5608 during the final thrust arc. This behavior demonstrates that during the first thrust arc the majority of the thrust is in the transverse direction in order to increase the size of the orbit since $a_f = 4.1642$ DU, which is much larger than $a_0 = 1.0980$ DU and that during the final thrust arc the majority of the thrust is in the transverse and normal directions to increase the size and the inclination of the orbit. Throughout the orbit transfer, the radial direction remains small compared to the other directions.

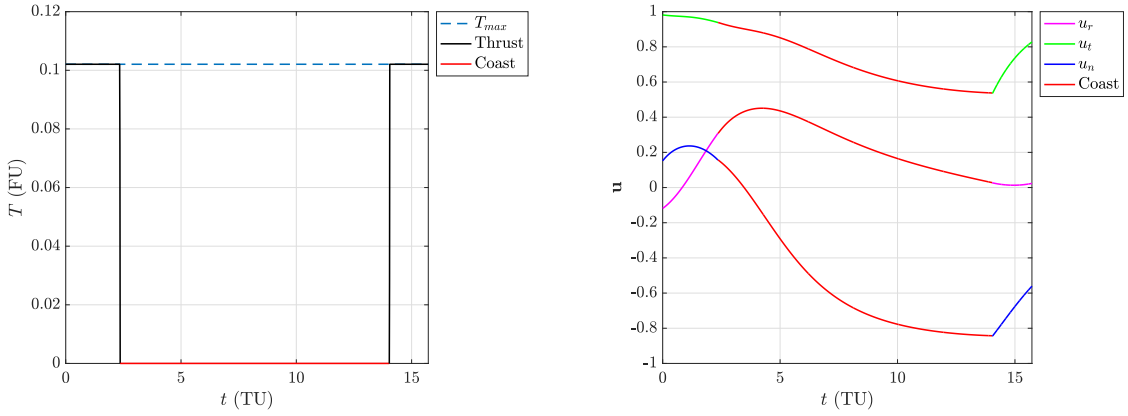

(a) Thrust magnitude.

(b) Thrust direction components.

Fig. 4 Control of the optimal trajectory.

2. Multiple Revolution Optimized Solution

Figure 5 shows the optimized three-dimensional trajectory of the LEO-to-MEO transfer for $s_0 = 1.0206 \times 10^{-3}$ AU in scaled Cartesian coordinates, where the conversion between modified equinoctial elements and position can be found in Ref. [16]. It is seen that the spacecraft begins in a low Earth orbit that corresponds to the orbital elements $(a_0, e_0, \Omega_0, i_0, \omega_0, \nu_0) = (1.0980 \text{ DU}, 0, 0 \text{ rad}, 0.4974 \text{ rad}, 0 \text{ rad}, \text{Free})$ and terminates in a middle Earth orbit that corresponds to the orbital elements $\left(a_f, e_f, \Omega_f, i_f, \omega_f, \nu_f\right) = (4.1642 \text{ DU}, 0, 0 \text{ rad}, 0.9547 \text{ rad}, \text{Undefined}, \text{Free})$.

The optimal trajectory consists of 31.6368 revolutions with a final mass of 0.5991 MU, four thrust arcs, and a total time thrusting of 487.3276 TU. It is seen that the spacecraft has four thrust arcs, where the coast arcs are near the end of the trajectory.

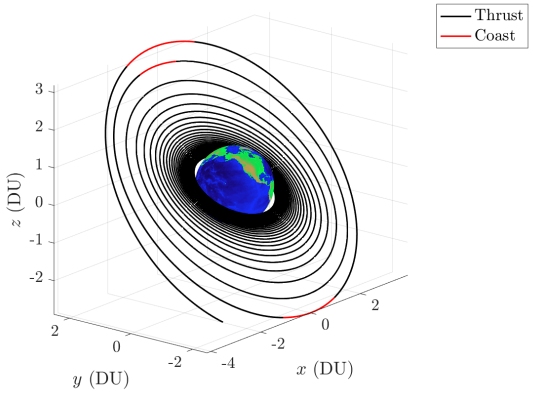

Fig. 5 Optimal three-dimensional spacecraft trajectory.

Figure 6 shows the behavior of the orbital elements of the optimized trajectory. The semi-major axis, a, steadily increases from 1.0980 DU to 4.1642 DU throughout the trajectory, with three small coast arcs near the end. The semi-major axis is always increasing because the trajectory of the spacecraft is always moving farther away from the Earth. The eccentricity, e, starts at 0 in accordance to the initial boundary conditions, then oscillates with increasing amplitudes around approximately 0.003 at the start of the trajectory and ends up oscillating around approximately 0.017, then terminates at 0, in accordance to the terminal boundary conditions. The eccentricity begins and ends at 0 because the initial and terminal orbits are circular and oscillates due to the multiple revolutions of the optimal trajectory. The right ascension of the ascending node, Ω, oscillates around 0 rad with increasing amplitudes, where it begins and ends at 0 rad. This behavior is a result of the boundary conditions for both the initial LEO and final MEO orbits, since it is required that $\Omega = 0$ rad at those points on the trajectory. It is also noted that the line of nodes moves only slightly since Ω has a range of 0.0219 rad. The inclination, i, increases from 0.4974 rad to 0.9547 rad, where the rate of change increases throughout the trajectory. The increasing rate of change for the inclination is more fuel efficient because the spacecraft is moving farther away from the Earth throughout the optimal trajectory, therefore the velocity is becoming smaller, and inclination changes require a change in the direction of velocity. Therefore, when the velocity is smaller the maneuver will require less fuel to be implemented, so the inclination changes more rapidly as the spacecraft moves farther away from the Earth. This behavior is because changing the inclination more rapidly when the spacecraft is farther away from the Earth is more fuel efficient since the velocity is smaller, and inclination changes require a change in the direction of velocity, so when the velocity is smaller the maneuver will require less fuel to be implemented. The argument of the periapsis, ω, is only undefined at the initial and terminal end points because $e = 0$, which explains the discontinuity that occurs at the end of the trajectory. For the defined portions of ω, it starts at 0 rad and terminates at 0.8069 rad, while oscillating around 0 rad with a range of 6.2775 rad. The true longitude, L, increases from -12.5664 rad to 186.2137 rad, where the rate of change is decreasing throughout the trajectory. It is noted that the true longitude rapidly increases during the beginning portion compared to the slow increase during the later portion because the velocity of the spacecraft is higher when it is located closer to Earth.

Figure 7 shows the mass of the spacecraft throughout the fuel-optimized trajectory. The mass starts at 1 MU, as in accordance with the initial boundary conditions, then decreases to 0.5991 MU, which is the optimized final mass, where the rate of change of mass is constant excluding the three short coast arcs. The amount of fuel consumed for the LEO-to-MEO transfer is 0.4009 MU.

Finally, Fig. 8 shows the control components of the optimal trajectory, which are the thrust magnitude, T, and the thrust direction components, (u_r, u_t, u_n). The thrust magnitude maintains a thrust of $T_{\max} = 1.021 \times 10^{-3}$ FU for most of the trajectory, with three short coast arcs near the end, therefore the thrust has six discontinuities and the structure of this solution is bang-off-bang-off-bang-off-bang. It is noted that the structure of the thrust is not assumed before solving the problem. The components of the thrust direction are only applicable when the thrust is non-zero (i.e., the four thrust arcs). The radial thrust direction, u_r, remains at approximately 0 for most of the trajectory, with a range of 0.1206.

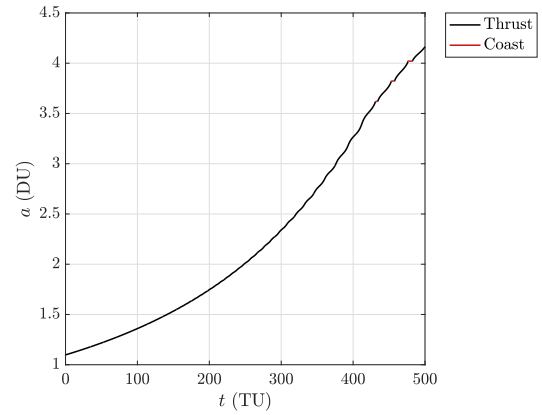

(a) Semi-major axis.

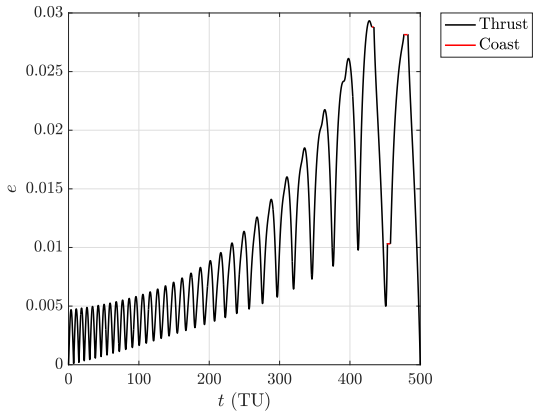

(b) Eccentricity.

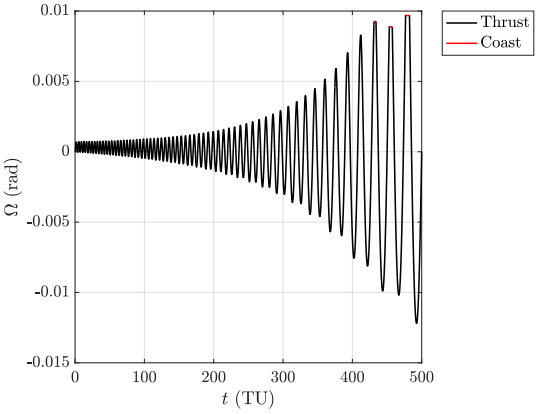

(c) Right ascension of the ascending node.

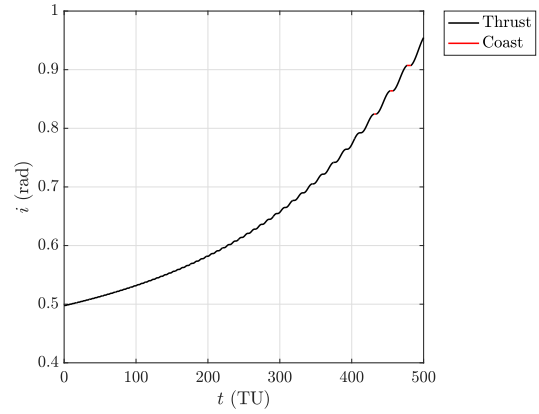

(d) Inclination.

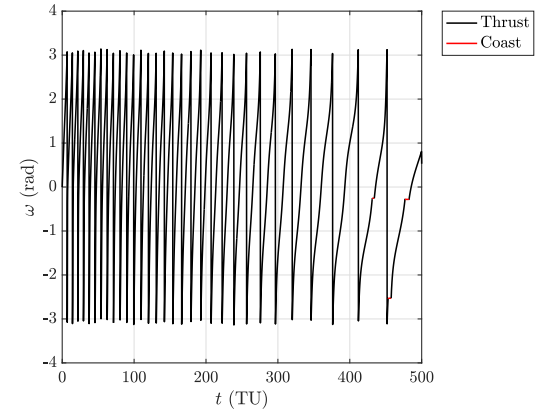

(e) Argument of the periapsis.

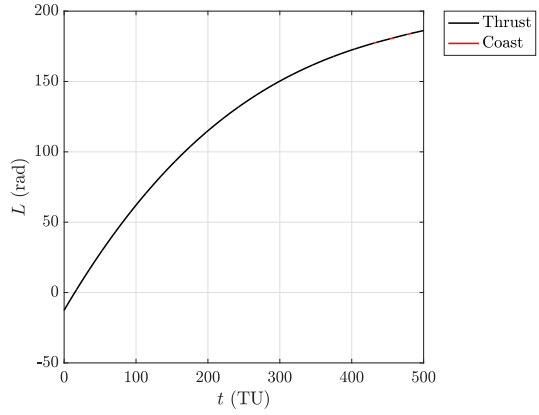

(f) True longitude.

Fig. 6 Orbital elements of the optimal trajectory.

The transverse thrust direction, u_t, oscillates around approximately 0.9 at the beginning and steadily decreases to then oscillate around approximately 0.6 at the end, with increasing amplitudes throughout and a range of 0.7648. The normal thrust direction, u_n, oscillates around 0 with increasing amplitudes throughout the trajectory, with a range of 1.9260. This behavior demonstrates that the majority of the thrust is in the transverse direction for most of the trajectory, in order

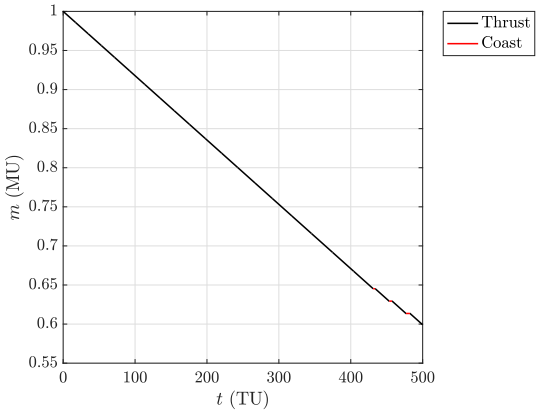

Fig. 7 Mass of spacecraft.

to increase the size of the orbit since $a_f = 4.1642$ DU, which is much larger than $a_0 = 1.0980$ DU. The normal direction starts to contribute more to the thrust direction during the later half of the trajectory because the inclination is changing more rapidly. Throughout the orbit transfer, the radial direction remains small compared to the other directions.

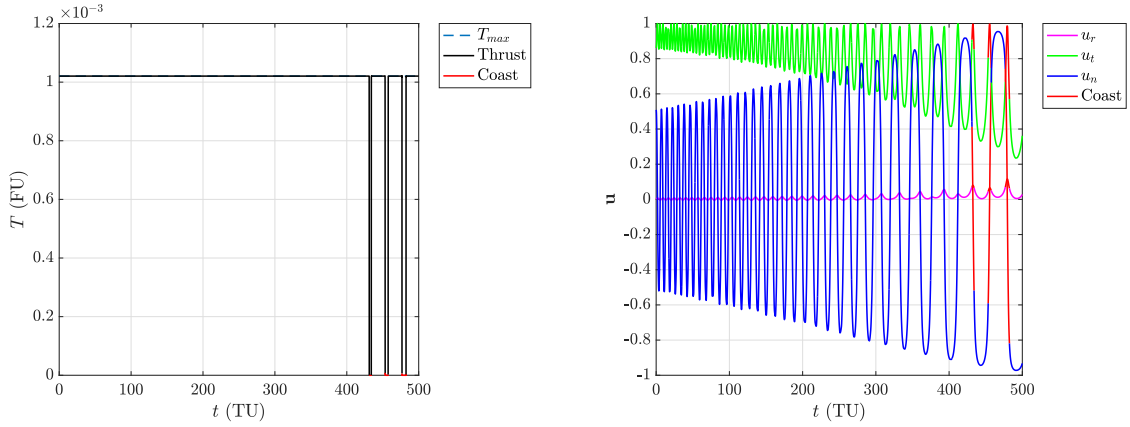

(a) Thrust magnitude.

(b) Thrust direction components.

Fig. 8 Control of the optimal trajectory.

IV. Conclusions

This research performed a numerical optimization study of a one-phase minimum-fuel LEO-to-MEO orbital trajectory transfer using a method to solve bang-bang optimal control problems and multi-domain Legendre-Gauss-Radau quadrature collocation. Seven cases of initial thrust acceleration values were considered. The time, t, state components, (p, f, g, h, k, L, m), and control components, (u_r, u_t, u_n, T) were optimized in this one phase problem. Numerical performance is improved by scaling the problem such that the Earth's gravitational parameter is unity. It was found that the solutions could be separated into two categories: partial and multiple revolution optimal trajectories. The initial thrust accelerations considered for the partial revolution solutions were $s_0 = \left[1.0206 \times 10^0, 5.1029 \times 10^{-1}, 1.0206 \times 10^{-1}, 5.1029 \times 10^{-2}\right]$ AU. Furthermore, as the initial thrust acceleration decreased, the final mass decreased, while naturally the amount of fuel consumed increased, and the total time thrusting increased. The initial thrust accelerations considered for the multiple revolution solutions were $s_0 = \left[1.0206 \times 10^{-2}, 5.1029 \times 10^{-3}, 1.0206 \times 10^{-3}\right]$ AU. Furthermore, as the initial thrust acceleration decreased, the

final mass increased, while naturally the amount of fuel consumed decreased, and the total time thrusting increased. An in-depth study was completed for the cases of $s_0 = \left[1.0206 \times 10^{-1}, 1.0206 \times 10^{-3}\right]$ AU. The final mass was $[0.4860, 0.5991]$ MU, the fuel consumed was $[0.5140, 0.4009]$ MU, the total time thrusting was $[4.0305, 487.3276]$ TU, the total amount of revolutions performed was $[0.6774, 31.6368]$, and the number of thrust arcs was $[2, 4]$.

Acknowledgments

The authors gratefully acknowledge support for this research from the U.S. National Science Foundation under grant DMS-1819002 and CMMI-2031213, the U.S. Office of Naval Research under grant N00014-19-1-2543, and the National Aeronautics and Space Administration under grant NNX15AI10H through the University of Central Florida NASA Space Grant Consortium and Space Florida.

References

[1] Morante, D., Sanjurjo Rivo, M., and Soler, M., "A Survey on Low-Thrust Trajectory Optimization Approaches," 2021.

[2] Starek, J. A., and Kolmanovsky, I. V., "Nonlinear model predictive control strategy for low thrust spacecraft missions," 2012.

[3] Dachwald, B., "Optimization of very-low-thrust trajectories using evolutionary neurocontrol," 2005.

[4] Jiang, F., Baoyin, H., and Li, J., "Practical Techniques for Low-Thrust Trajectory Optimization with Homotopic Approach," *Journal of Guidance, Control, and Dynamics*, Vol. 35, No. 1, 2012, pp. 245–258. https://doi.org/10.2514/1.52476, doi:10.2514/1.52476.

[5] Rauwolf, G. A., and Coverstone-Carroll, V. L., "Near-Optimal Low-Thrust Orbit Transfers Generated by a Genetic Algorithm," 1996.

[6] Coverstone-Carroll, V., Hartmann, J. W., and Mason, W. J., "Optimal multi-objective low-thrust spacecraft trajectories," *Computer Methods in Applied Mechanics and Engineering*, Vol. 186, No. 2–4, 2000, pp. 387–402. https://doi.org/10.1016/S0045--7825(99)00393--X, doi:10.1016/S0045-7825(99)00393-X.

[7] Graham, K., and Rao, A., "Minimum-Time Trajectory Optimization of Multiple Revolution Low-Thrust Earth-Orbit Transfers," 2015.

[8] Betts, J. T., "Optimal low-thrust orbit transfers with eclipsing," 2014.

[9] Lee, D., "Minimum-Fuel Planar Earth-to-Mars Low-Thrust Trajectories Using Bang-Bang Control," , 2021. URL https://www.preprints.org/manuscript/202109.0226/v1.

[10] Gergaud, J., and Haberkorn, T., "Homotopy method for minimum consumption orbit transfer problem," 2006.

[11] Herman, A. L., and Spencer, D. B., "Optimal, Low-Thrust Earth-Orbit Transfers Using Higher-Order Collocation Methods," *Journal of Guidance, Control, and Dynamics*, Vol. 25, No. 1, 2002, pp. 40–47. https://doi.org/10.2514/2.4873, doi:10.2514/2.4873.

[12] Pager, E. R., and Rao, A. V., "Method for Solving Bang-Bang and Singular Optimal Control Problems using Adaptive Radau Collocation," , 2021. URL https://arxiv.org/pdf/2104.12247.pdf.

[13] Biegler, L. T., and Zavala, V. M., "Large-Scale Nonlinear Programming Using IPOPT: An Integrating Framework for Enterprise-Wide Dynamic Optimization," *Computers and Chemical Engineering*, Vol. 33, No. 3, 2009, pp. 575–582. https://doi.org/10.1016/j.compchemeng.2008.08.006, doi:10.1016/j.compchemeng.2008.08.006.

[14] Herman, A. L., "Improved Collocation Methods with Application to Direct Trajectory Optimization," , Sept. 1995.

[15] Spencer, D. B., "An Analytical Solution Method for Near-Optimal Continuous-Thrust Orbit Transfers," , 1994.

[16] NASA, J., "Modified Equinoctial Elements," , 2005. URL https://spsweb.fltops.jpl.nasa.gov/portaldataops/mpg/MPG_Docs/Source%20Docs/EquinoctalElements-modified.pdf.

[17] Betts, J. T., *Practical Methods for Optimal Control and Estimation Using Nonlinear Programming*, Society for Industrial and Applied Mathematics, 2010.

[18] Patterson, M. A., and Rao, A. V., "GPOPS-II: A MATLAB Software for Solving Multiple-Phase Optimal Control Problems Using hp-Adaptive Gaussian Quadrature Collocation Methods and Sparse Nonlinear Programming," *ACM Transactions on Mathematical Software*, Vol. 41, No. 1, 2014, pp. 1:1–1:37. https://doi.org/10.1145/2558904, doi:10.1145/2558904.

[19] Patterson, M. A., Hager, W. W., and Rao, A. V., "A ph Mesh Refinement Method for Optimal Control," *Optimal Control Applications and Methods*, Vol. 36, No. 4, 2015, pp. 398–421. doi:10.1002/oca.2114.

[20] Weinstein, M. J., and Rao, A. V., "Algorithm 984: ADiGator, a Toolbox for the Algorithmic Differentiation of Mathematical Functions in MATLAB Using Source Transformation via Operator Overloading," *ACM Transactions on Mathematical Software*, Vol. 44, No. 2, 2017, pp. 21:1–21:25. https://doi.org/10.1145/3104990, doi:10.1145/3104990.